## Title

Motion-robust, multi-slice, real-time MR thermometry for MR-guided thermal therapy in abdominal organs.



## Journal

International journal of hyperthermia : the official journal of European Society for Hyperthermic Oncology, North American Hyperthermia Group, 40(1)

## ISSN

0265-6736

## Authors

Kim, Kisoo
Diederich, Chris
Narsinh, Kazim
et al.

## Publication Date

2023

## DOI

10.1080/02656736.2022.2151649

Title Page

Title:

# Motion-robust, multi-slice, real-time MR thermometry for MR-guided thermal therapy in abdominal organs

Authors: Kisoo Kim[1*], Chris Diederich[2], Kazim Narsinh[1], Eugene Ozhinsky[1]
1. Department of Radiology & Biomedical Imaging, University of California, San Francisco, USA
2. Department of Radiation Oncology, University of California, San Francisco, USA

Subheadings: Motion-robust MR thermometry in abdominal organs

Word count (without reference and abstract): 5119

*Correspondence:
Kisoo Kim, Ph.D.
Department of Radiology & Biomedical Imaging
University of California, San Francisco
2340 Sutter Street, S341,
94115 San Francisco, California, USA
415-260-5978
ki-soo.kim@ucsf.edu

**Abstract**

**Purpose:** To develop an effective and practical reconstruction pipeline to achieve motion-robust, multi-slice, real-time MR thermometry for monitoring thermal therapy in abdominal organs.

**Methods:** The application includes a fast spiral MRI pulse sequence and a real-time reconstruction pipeline based on multi-baseline proton resonance frequency shift (PRFS) method with visualization of temperature imaging. The pipeline supports multi-slice acquisition with minimal reconstruction lag. Simulations with a virtual motion phantom were performed to investigate the influence of the number of baselines and respiratory rate on the accuracy of temperature measurement. Phantom experiments with ultrasound heating were performed using a custom-made motion phantom to evaluate the performance of the pipeline. Lastly, experiments in healthy volunteers (N=2) without heating were performed to evaluate the accuracy and stability of MR thermometry in abdominal organs (liver and kidney).

**Results:** The multi-baseline approach with greater than 25 baselines resulted in minimal temperature errors in the simulation. Phantom experiments demonstrated a 713 ms update time for 3-slice acquisitions. Temperature maps with 30 baselines showed clear temperature distributions caused by ultrasound heating in the respiratory phantom. Finally, the pipeline was evaluated with physiologic motions in healthy volunteers without heating, which demonstrated the accuracy (RMSE) of 1.23±0.18°C (liver) and 1.21±0.17°C (kidney) and precision of 1.13±0.11°C (liver) and 1.16±0.15°C (kidney) using 32 baselines.

**Conclusions:** The proposed real-time acquisition and reconstruction pipeline allows motion-robust, multi-slice, real-time temperature monitoring within the abdomen during free breathing.

**Keywords:** MR thermometry, abdominal organ, motion, real-time MR imaging, MR-guided thermal therapy

## 1. Introduction

Magnetic Resonance Imaging (MRI) offers inherent advantages for the guidance of thermal therapy for tumor treatments. MRI allows real-time, non-invasive temperature monitoring for treatment control and patient safety, as well as superior soft tissue contrasts for treatment planning. Although various MRI parameters[1] are sensitive to relative changes in temperature, a phase-based proton resonance frequency shift (PRFS) method for MR thermometry is the most commonly used for clinical MR-guided thermal therapy due to its fast acquisition and high-temperature sensitivity.[2,3] The PRFS method is based on measuring the phase difference between phase images at two different time points, which allows for calculating the relative change in tissue temperature. Currently, clinical MR-guided focused ultrasound ablation systems using the PRFS method have been FDA-approved for thermal ablation treatment of prostate, uterine fibroids, bone metastases, and brain (Essential tremor and Parkinson's disease).[4] Additionally, other heating techniques, such as microwave, RF, and laser, have been used with the PRFS MR thermometry to treat localized tumors in sites, such as the liver, kidney, brain, and prostate.[5–9]

When imaging moving organs, intra-frame motion adversely impacts the quality of PRFS-based MR thermometry. The PRFS method has the highest temperature sensitivity when an echo time (TE) is the same or closest to the $T_2$* relaxation time in tissue. The echo time often needs to be longer than other real-time MRI sequences. In the case of using a spoiled gradient echo sequence, this naturally increases a repetition time (TR) and thus can be more vulnerable to intra-frame motion. To enable a higher frame rate and reduce intra-frame motion, rapid pulse sequences with echo-planar length (EPI) and/or spiral readout trajectories have been investigated for real-time MR PRFS thermometry.[10–12]

The PRFS reconstruction method is based on phase subtraction and is very sensitive to motion due to misregistration between phase images and changes in magnetic susceptibility. For monitoring MR-guided thermal therapies in moving abdominal organs, a number of approaches have been developed to enable real-time MR PRFS thermometry using rapid pulse sequences. Multi-baseline acquisitions work by acquiring a library of baseline images during the cardiac or breathing cycles and matching images acquired during heating to the closest baseline before phase subtraction.[13–15] Hey et al[14] proposed the model-based MR thermometry motion correction. With a rapid estimation of the diaphragm position based on the image phase, they demonstrated that the model-based correction improved the temperature precision by 16-36 % compared to the look-up-table-based correction in the breast of healthy volunteers. A referenceless method has been proposed as another option for motion-robust PRFS temperature mapping.[16,17] A polynomial fitting from the background phase outside the heated region can provide the phase estimate in the heated region, and enables the PRFS calculation with a single-phase image. Grissom et al. combined multi-baseline and referenceless approaches to develop hybrid MR thermometry for monitoring thermal therapies in moving organs.[18] Other approaches for motion-robust MR thermometry have been proposed, such as using principal component analysis[19], phase navigators[20,21], and deep-learning correction[22]. Recently, de Senneville et al.[22] extended the multi-baseline approach using deep learning to correct temperature errors due to motion-induced phase variations and time-variant magnetic fields. Their workflow minimized inherent computational costs with pre-procedure training of

convolutional neural network during free-breathing and enabled following the temperature evolution of an in-vivo HIFU ablation.

These existing approaches have the potential for practical use in clinical MR-guided thermal therapies, however, there are inherent tradeoffs between computational costs, spatial coverage, and precision of temperature measurement. A fast-imaging frame rate (e.g., ~300 ms) allows for minimizing intra-frame motion artifacts during MR acquisition and performing a multi-slice acquisition, while this naturally increases the computational burden when applying a complex algorithm to correct motion artifacts. Additionally, continuous reconstruction of MR thermometry data may be limited by high computation costs and reconstruction lag. A significant measurement delay is introduced when the MRI images are initially stored as files before being transferred and further processed to generate temperature maps. Roujol et al.[23] developed a computationally effective processing pipeline for real-time MR thermometry in abdominal organs by using a CPU/GPU architecture to process a displacement estimation and an MR thermometry correction within a few milliseconds (i.e., 27.3 ms). This processing pipeline was shown to provide a temporal resolution of 100 ms with a precision of less than 2 °C within an ROI in the kidney and liver for 5 min. Celicanin et al.[24] developed motion correction methods for focused ultrasound ablation using a segmented EPI-based MR pulse sequence with pencil beam navigators. With real-time motion tracking, an MR thermometry slice was readjusted during sonication. The referenceless reconstruction method was applied for motion correction. The EPI-based MR sequence and their processing pipeline could provide thermometry visualization every 1 s per slice with a high spatial resolution (1.5 mm x 1.5 mm x 5 mm), while the temperature was measured only within a small ROI in a single slice due to the referenceless method and the purpose of thermal ablation. More detailed reviews on motion-insensitive MRI acquisitions and practical considerations are given by Winter et al.[25] and Odéen et al.[26]

The objective of this study was to develop an effective and practical processing pipeline for multi-slice, motion-robust, and real-time MR thermometry using a real-time MRI research platform. This pipeline with the multi-baseline approach was designed to maximize computational acceleration, spatial coverage, and precision of temperature measurement while minimizing image artifacts and reconstruction lag. The pipeline and real-time MR thermometry application were developed using the RTHawk research platform (HeartVista, Inc.).[27] The RTHawk platform featured a virtual MRI simulation, real-time image visualization, and development tools to develop custom sequences and acceleration schemes. A virtual simulation phantom within RTHawk was used to evaluate the accuracy of temperature measurement according to the number of baselines. Experiments were performed with a previously developed pneumatic respiratory motion phantom and ultrasound heating in order to evaluate the practical performance of the pipeline. Finally, experiments in healthy volunteers were performed without heating to evaluate the stability and accuracy of temperature measurement in the presence of physiological motion in abdominal organs, tracking ROIs in the kidney and liver.

## 2. Methods

### 2.1 Real-time MRI Pulse Sequence

A spectral-spatial RF pulse for water-only excitation has been shown in real-time MR

PRFS thermometry to reduce temperature errors induced by fat[28–30] and also to improve the quality of MR thermometry in abdominal organs.[28] In this study, a 1-2-1 binomial sub-pulse RF excitation was used as a spectral-spatial RF pulse and its excitation length was set up at approximately 6 ms. For the readout sequence, a spiral-out trajectory allowed achieving higher temporal resolution than fully-sampled Cartesian readout in MR thermometry.[30] The readout parameters were the readout length=10.7 ms and the number of interleaves=11. A rapid 1-dimensional pencil-beam navigator sequence with an acquisition time of 17 ms was interleaved with the thermometry sequence to track respiratory motion.

### 2.2 Real-time Reconstruction Pipeline for Multi-baseline PRFS Thermometry

The pulse sequence and reconstruction pipeline were developed on the RTHawk Research Platform (HeartVista, Menlo Park, CA). An accelerated GRE sequence was designed including a spectral-spatial RF pulse and a spiral readout trajectory. A multi-baseline reconstruction pipeline was developed for the correction of motion artifacts in PRFS measurements (Figure.1a). Multi-slice images and navigator data were continuously acquired and processed in the multi-baseline reconstruction pipeline (Figure 1b). The application allowed defining the acceptance window for navigator positions to be mapped to multiple branches of the reconstruction pipeline according to baseline numbers and respiration phases. Figure 1c shows an example of a multi-baseline acquisition with five respiratory positions for inhale phase and five for exhale phase.

The change in real-time displacement measurements was used to distinguish between inhalation and exhalation respiration phases through comparison with previous and current navigator positions. After obtaining a respiration phase, raw k-space data was routed according to respiratory phase and navigator position so that the current dynamic and baseline images, acquired at similar navigator positions and respiration phases, were passed through the same branch of the pipeline in order to minimize motion-induced temperature errors. In each branch of the pipeline, gridding reconstruction from the under-sampled spiral k-space trajectory data was performed. A commercial 4-channel spine coil and 8-channel cardiac coil were used for experiments with phantom/volunteer #1 and volunteer #2, respectively. For these multi-channel array coils, each branch had multiple pipelines for data from each channel. Complex MR signals from each coil were combined to acquire the weighted average of phases using a vendor-supplied “complex sum” function (RTHawk). After the PRFS reconstruction, the temperature maps were visualized continuously in real-time. The magnitude images were reconstructed using the sum-of-square approach to combine complex images from multiple coils.

Before the start of heating, baseline images were recorded until 30 or more baselines covering over 90% of the positions of the organ (i.e., 90% of the branches) were available. Processing time can vary based on the subject’s motion amplitude and patterns. Only the pipeline branches that recorded baseline data were activated. Afterward, during temperature monitoring, only the images corresponding to active pipeline branches were processed through the reconstruction pipeline and visualized in the user interface. Data from the branches that did not record baseline images was discarded. The RTHawk software was installed on a workstation operating Ubuntu 20.04 LTS system (2.4GHz, 16

processors, and 64 GB RAM).

### 2.3 Virtual Phantom Simulation

The developed MR thermometry application was evaluated in a simulation with a virtual respiratory motion phantom integrated with the RTHawk Platform (Figure 2a). The virtual phantom can simulate a respiratory motion with various respiratory rates. In the simulation, raw k-space data was created based on an MRI pulse sequence, and the data was processed through the reconstruction pipeline. Although this simulation does not provide electromagnetic properties such as $T_1$ and $T_2$ relaxation time, misregistration between phase images in the PRFS calculation can be simulated. Thus, the proposed pipeline could be tested with various control parameters such as the acquisition time and the number of baselines. The accuracy and precision of temperature measurements (see section 2.6) were evaluated with varying baseline numbers and respiratory rates.

A single axial slice was set at the center of the phantom and PRFS temperature maps at each baseline were collected for 60 s. MR parameters included TR = 22.5 ms, TE = 11 ms, Field of view (FOV) = 400 $mm^2$, thickness = 5 mm, total acquisition time per slice (including the navigator sequence) = 264.5 ms. The pencil beam navigator sequence included: dimension = 3.0 cm x 3.0 cm x 14.7 cm and acquisition time=17 ms. A window of the pencil beam navigator was placed on the surface of the phantom in an axial plane and measured the displacement of the virtual phantom.

### 2.4 Experiments with a respiratory motion phantom

#### 2.4.1 Respiratory motion phantom

The previously developed motion phantom was used for this study to mimic respiratory-induced organ motion.[31] This low-cost MR-compatible respiratory motion simulator included two main processes: 1) outside the MRI suite a DC motor of 16 cycles/min was connected to a motion actuator, which increased or decreased the pressure inside the bag valve mask (BVM). 2) The BVM was coupled via Tygon tubing to the compressible bag in the motion phantom in the MRI scanner (Figure 2b). Various levels of inflation or deflation of the BVM caused the cyclical motion of a tissue-mimicking phantom in the MRI scanner to simulate the shift of abdominal organs due to respiratory motion. The tissue-mimicking phantom was placed on the plastic holder with wheels (integrated with the motion simulator), and the motion simulator generated a cyclical motion of approximately 7.5 mm along the axis of the MRI bore to simulate an organ motion. Details about the custom-made motion simulator are shown in Supporting Material Figure S1.

An MR-compatible piezoceramic transducer (EBL Products Inc., USA) and assembly were used to add ultrasound heating to the motion phantom. A 31.75 mm × 31.75 mm square transducer was mounted on a 3D printed housing and sealed with silicone adhesive to maintain air-backing. RG174 coaxial cable, soldered to each electrode surface, was connected on the control room side of the penetration panel to a low-pass RF filter for suppression of RF harmonics, in series with an ENI RF 240L amplifier (BELL Electronics NW, Inc, USA) controlled by a function generator (Agilent Technologies, Inc., USA). The transducer was operated at 3.4 MHz at an acoustic output intensity of approximately 2.4 $W/cm^2$.

### 2.4.2 Experimental Protocols

There were two experimental protocols for evaluating the pipeline with the respiratory phantom. All experiments were performed with a 3T MRI scanner (GE Healthcare, Discovery MR750W, Waukesha, WI). In the first experiment, a tissue-mimicking phantom (InSightec, Israel) was used with the motion phantom to evaluate the temperature stability over 190 s of multi-slice acquisition without heating. Three contiguous coronal slices were acquired over 3:10 min and multi-baseline images were collected with 30 phases of the simulated breathing cycle for 1:40 min before the scanning. The MRI parameters included number of slices = 3, TR/TE = 21.1/10 ms, matrix = 158 × 158, thickness = 5 mm, FOV = 240 $mm^2$, 3 coronal slices, and total acquisition time per 3 slices (including the navigator sequence) = 713.3 ms.

In the second set of experiments the ultrasound transducer, in a fixed position at the bottom of the container beneath the oscillating phantom, was used to apply a realistic heating distribution within the phantom and thus allow evaluation of the performance of the pipeline to monitor temperature during movement (Figure 2b). 30 baselines over the breathing cycle were used in this experiment and were recorded for 50 s before the heating. The MRI parameters included TR/TE = 26/14.78 ms, matrix = 158 × 158, thickness = 5 mm, FOV = 240 $mm^2$, a single slice, and total acquisition time per slice = 303 ms. Coronal slices were acquired for 205 s. The pencil beam navigator was prescribed over the center of the phantom in a coronal plane to track the movement.

## 2.5 Experiments in Healthy Volunteers

Experiments in two healthy volunteers without heating were implemented to evaluate the stability of temperature measurements with free-breathing and physiological motion, as approved by the institutional review board (IRB) at the University of California, San Francisco (IRB number: 11-08177). The liver and left/right kidney were measured with coronal and axial images (Table 1). Multi-baseline MR images were acquired at 32 phases of the breathing cycle. Baselines were recorded over a 1 min interval, then the temperature monitoring was applied for 70-170 s. The MRI parameters included TR/TE = 22.2/11 ms, matrix = 158 × 158, thickness = 5 mm, and FOV = 450-530 $mm^2$. The total acquisition time per slice was 261.2 ms. The respiratory motion was measured by the pencil-beam navigator, with navigators positioned on the boundary between the diaphragm and liver in the inferior-superior direction.

## 2.6 Data Analysis

In this study, the root mean square error (RMSE) was calculated on a voxel-by-voxel basis over scan time, and then averaged within an ROI to assess the accuracy of MR thermometry obtained from the developed pipeline. For the stability of temperature measurements, the temporal standard deviation was calculated on a voxel-by-voxel basis over time and averaged within an ROI.

To compare multi-baseline and single baseline reconstructions, the raw MRI datasets from all experiments were recorded and reconstructed offline using Matlab (MathWorks, Natick, MA). A PRFS calculation was performed using a single baseline image and was compared with the temperature maps, acquired with the real-time multi-baseline PRFS pipeline. This work allowed comparison between the PRFS

reconstruction methods on the same underlying data, avoiding variability due to differences in motion and heating conditions.

## 3. Results

### 3.1 Virtual Phantom Simulation

The simulations were performed to investigate the influence of the number of baselines and respiratory rates on temperature errors, uniformity, and stability. Figure 3a shows the comparison of MR thermometry between single baseline and multi-baseline PRFS acquisitions. The respiratory motion of the virtual phantom produced periodic thermometry artifacts observed in the temperature maps from single baseline PRFS reconstruction, while the multi-baseline reconstruction resulted in more homogeneous temperature maps with fewer artifacts throughout the breathing cycle.

In the simulation for varying baseline numbers, the temperature accuracy and precision in a single baseline acquisition were measured at 0.44 °C and 0.38 °C, respectively, and then normalized to 1 for comparison to values for an increasing number of baselines. Figure 3b shows a baseline of 25 or higher is likely to have similar temperature corrections at 12 cycles/min. Reconstruction with 25 or more baselines resulted in 17-20% accuracy in single baseline PRFS reconstruction.

Figure 3c shows the accuracy and precision of temperature measurement according to various respiratory rates. 25 baselines were used for the PRFS reconstruction, except for no motion case (single baseline). The temperature accuracy and precision without motion were measured at 0.0187 °C and 0.0185 °C, respectively, and then normalized to 1. Figure 3c shows that the temperature accuracy and precision are worsening at a respiratory rate higher than 12 cycles/min.

### 3.2 MRI experiments with the respiratory motion phantom

#### 3.2.1 Multi-slice MR thermometry without heating

Figure 4 compares PRFS temperature maps from single baseline and multi-baseline reconstruction within the respiratory phantom. The temperature maps for 3 slices were updated every 713.3 ms over the 3.75 s simulated breathing cycle. Similar to the simulation study, a single baseline acquisition produced large motion artifacts in temperature maps. In contrast, multi-baseline reconstruction mitigated motion artifacts in temperature maps and provided uniform and homogeneous temperature maps throughout the breathing cycle.

Time-dependent profiles of the temperature within an ROI are plotted in Figure 5 in 713.3 ms intervals over 190 s overall time frame. The multi-baseline reconstruction allowed stable and uniform temperature measurements at each slice, while a single baseline reconstruction showed periodic patterns corresponding to errors associated with the respiratory motion. The measured average RMSE in the multi-baseline acquisition for 190 s was 0.84 °C (slice 1), 0.84 °C (slice 2), and 0.81 °C (slice 3), compared to 1.44 °C (slice 1), 1.16 °C (slice 2), and 1.28 °C (slice 3) in a single baseline acquisition. In addition to accuracy, the precision was measured in the multi-baseline acquisition at 0.77 °C (slice 1), 0.75 °C (slice 2), and 0.72 °C (slice 3) compared to 1.40 °C (slice 1), 1.12 °C (slice 2), and 1.11 °C (slice 3) in a single baseline acquisition.

### 3.2.2 Single-slice MR thermometry with ultrasound heating

Figure 6 shows PRFS temperature maps obtained with ultrasound heating during phantom motion over a 205 s time course. The single baseline PRFS temperature maps suffered from motion-induced susceptibility artifacts and image misregistration between baseline and dynamic images, while the multi-baseline reconstruction produced homogeneous and stable temperature measurements. Time-dependent profiles of temperature were plotted with ROI 1 placed within the heated region and ROI 2 outside of the heated region toward the periphery. The multi-baseline reconstruction could generate stable and uniform temperature measurements within both ROI 1 and 2. Outside of the heated region (ROI 2), the measured average temperature was -0.24±0.2 °C for 205 s using the respiratory motion phantom. The averaged RMSE and precision in the multi-baseline acquisition were measured to be at 1.57 °C and 1.51 °C, respectively, while those in a single baseline acquisition were 2.78 °C and 2.76 °C, respectively. To investigate the field drift at the end of the scan the linear regression model was applied, and the temperature was estimated to be -0.4 °C at the end of the scan. The slope of the temperature profile over time within the ROI was measured to be -0.002 °C/s and the y-intercept to be -0.06 °C.

### 3.3 Experiments in Healthy Volunteers

The real-time multi-baseline thermometry pipeline was evaluated in two experiments with free-breathing human subjects without heating. The resulting PRFS temperature maps with single- and multi-baseline reconstruction are shown in Figure 7. The kidney had a maximum displacement of 15 mm along the cranio-caudal direction. Misregistration in the PRFS calculation and motion-induced susceptibility artifacts affected PRFS temperature maps with a single baseline, while it was significantly mitigated in those with multi-baseline reconstruction and homogeneous temperature distributions could be observed (Supporting Material Video S1). Time-dependent profiles of temperature within ROIs in the kidney indicated the stability of temperature measurement over the 74 s measurement interval. Periodic patterns corresponding to the respiratory motion were observed in PRFS temperature maps with a single baseline reconstruction, but not observed in those with the multi-baseline reconstruction (Figure 8). In time-dependent profiles, the temperature within an ROI was measured at -0.48±0.84 °C over 137 s (liver) and 0.39±0.88 °C over 170 s (kidney) in the multi-baseline acquisition. The averaged accuracy of 1.23±0.18 °C (liver) and 1.21±0.17 °C (kidney) and precision of 1.13±0.11 °C (liver) and 1.16±0.15 °C (kidney) were measured in the multi-baseline acquisition across two healthy volunteers, while the accuracy of 5.19±3.83 °C (liver) and 4.02±1.11 °C (kidney) and precision of 4.88±4.1 °C (liver) and 2.65± 0.62 °C (kidney) were measured in a single baseline acquisition (See Table 1 and Supporting Material Figure S3).

## 4. Discussion

In this study, an effective and practical reconstruction pipeline and real-time MR application were developed in this study to provide motion-robust, multi-slice, and real-time MR thermometry in abdominal organs. The result of experiments demonstrated that temperature maps reconstructed from the pipeline can provide stable and accurate temperature measurement in the phantom with simulated respiratory motion and in healthy volunteers with free breathing.

A spiral-based MRI sequence has been previously demonstrated as an effective acceleration for volumetric MR thermometry.[12,30] In this study, the spiral MR sequence specific for abdominal imaging was applied and allowed frame rates up to 4 frames per second (fps). Based on the result of experiments herein, 3.3-4 fps rates may be enough to minimize intra-frame motion artifacts that can occur if the acquisition time per frame is not fast enough. In addition to the frame rate, the current dynamic and baseline images in the multi-baseline PRFS method may have a similar extent of intra-frame artifacts due to being acquired at the same motion position. This may be also able to mitigate intra-frame motion artifacts.

In this study, the spiral MR sequence with 11 interleaves was used with a matrix size of 158 x 158 and FOV of 240 $mm^2$ (phantom) and 450-530 $mm^2$ (healthy volunteers). In experiments with both the motion phantom and healthy volunteers, these parameters allowed achieving the accuracy and precision of temperature measurement close to 1 °C. These results demonstrate the proposed reconstruction pipeline can provide a similar or better performance of MR thermometry in abdominal organs, compared to previous motion-robust MR thermometry studies.[14–16,18–20] Fielden et al. reported on the spiral in-out readout trajectory can offer a longer TE and blurring correction, which can result in more precise temperature measurements.[30] Although the spiral in-out readout approach was not used here, it can be easily incorporated into the proposed reconstruction pipeline.

The pencil beam navigator sequence has been often used for real-time motion correction in MR thermometry due to its fast and robust motion tracking capabilities.[15,24] The integrated pencil beam navigator sequence was interleaved with the thermometry sequences in our study, and only required 17 ms to measure tissue displacement. The navigator sequence allowed a respiratory motion to be measured directly without the need for complicated computational methods for displacement estimation or additional hardware. Correct placement of the navigator window was of the utmost importance to properly measure a breathing motion. In healthy volunteer experiments, the navigator window was located at the boundary of the diaphragm (case of the coronal slice) and the boundary of skin in the upper abdomen (case of the axial slice). This placement produced a clear measurement of breathing motion with the least amount of noise within the imaging plane.

In this study, virtual simulations of respiratory motion in RTHawk were performed to investigate the influence of the number of baselines and respiratory rates on temperature measurements in the presence of periodic motion. Our results showed that the reconstruction with 25 or higher number of baselines resulted in the temperature images with the least amount of errors (Figure 3b). Therefore, we have chosen to use 30 or more baselines for MR thermometry reconstruction in phantom and in-vivo experiments. We also investigated the change in the accuracy and precision of temperature measurements over a range of respiratory rates. Note that temperature errors in the simulation were only caused by misregistration between two phase images, and did not include magnetic susceptibility artifacts. Although the simulation environment was limited, the results showed the temperature accuracy and precision worsened at respiratory rates higher than 12 cycles/min.

The multi-baseline approach requires collecting the baseline library before the treatment. The thermometry pipeline and graphic user interface in the RTHawk

platform featured an automated baseline set up from a navigator window, a display of recording status, and the number of acquired baselines (Supporting Material Figure S2). After recording baseline data, unused branches of the pipeline were disabled so that recorded baselines were only used for temperature reconstruction. This function may result in a more stable temperature measurement by avoiding passing through the wrong branch of the pipeline. In this study, we stopped recording baselines when a recording status reached the condition satisfying both more than 30 baselines and 90% of positions. A gap in temperature measurement may occur due to discarded images. We observed that discarded images, which were not matched to baselines, were less than 3% of the total acquired images. Thus, it did not significantly affect the performance of real-time monitoring. Furthermore, this filtering allowed our multi-baseline reconstruction to minimize temperature errors even in case of somewhat unstable motion patterns in the healthy volunteers.

The multi-baseline approach has an intrinsic limitation, which requires periodic motion and does not help with other types of motion, such as bulk, bowel, and intestinal gas motion. To correct susceptibility artifacts induced by those types of motion, a recent study proposed a method for susceptibility artifact correction using the total field inversion approach.[32] They demonstrated that the approach allowed a stable temperature estimation in the pelvic region. However, the computation time for one image required more time than other previous approaches and a need for high-performance GPU/CPU hardware for processing. In addition, the multi-baseline approach cannot correct for the errors induced by tissue deformation and heat-induced tissue swelling after recording of the baseline data.[26]

Our approach has several technical limitations. First, we used a single navigator sequence in the pipeline even when performing the multi-slice acquisition. Therefore, the amount of actual tissue displacement may be different for each slice. In our experiments, 713 ms of acquisition time for 3 slices provided the temperature accuracy and precision of less than 1 °C over the 3.75 s simulated breathing cycle (16 cycles/min) while motion patterns were stable. In order to improve accuracy for multi-slice acquisition in unstable motion patterns, further study could investigate the use of multiple navigators to record a baseline associated with each slice.[33] Second, artifacts in a certain region of the abdomen were observed. The pulsatile blood flow hampered temperature estimation in the region close to major blood vessels, as noted there is no compensation for flow artifacts built into our pipeline (Supporting Material Figure S3). Our approach may be combined with other MR compensation techniques such as a saturation MRI pulse to eliminate unwanted flow artifacts, which may potentially increase scan time, while it may allow a stable temperature measurement close to these major vessels. Finally, out-of-plane organ motion may negatively affect the accuracy of continuous temperature measurements. In healthy volunteer experiments, we observed organ motion dominantly along the SI direction, with the coronal slice being the best for monitoring the liver and kidney. However, when organs moved out of the image plane, a spike in temperature error was observed. To minimize these spikes, future studies may include a 3D motion compensation using the slice-tracking technique.[33]

This study focused on the development and initial evaluation of a novel MR thermometry reconstruction technique. Thus, our experimental design had several

practical limitations. First, our experiments on the phantom and in vivo with healthy volunteers had acquisition durations of 70-205 s. Clinical hyperthermia treatments will require temperature imaging for longer durations (10-90 mins). To validate our thermometry application for hyperthermia monitoring, further study is needed to measure temperature accuracy at prolonged heating durations. Field drift is often a problem in long-term MR thermometry acquisitions with some MRI sequences. The field-drift correction is commonly used to correct the main magnetic field drifts over these long durations. In this study, we did not observe large temperature errors resulting from the main magnetic field drifts, so real-time drift correction was not applied. We determined the slope of the temperature profile over scan time within ROI 2 using linear regression. As a result, the temperature error induced by the field-drift was estimated as -0.4 °C with the slope of -0.002 °C/s and the y-intercept of -0.06 °C in the linear regression model. We thus assumed no significant field drifts in all experiments presented here. If a large field drift is detected, e.g., more than 1 °C outside the heating region, the correction can be easily applied during post-processing.[34] Finally, we performed in-vivo human experiments without any heat delivery for safety reasons. Future studies with in-vivo animal models should be performed to evaluate the performance of our approach while heating moving organs.

Major MRI system vendors provide interactive MR imaging environments, allowing dynamic control of MR parameters and reconstruction: Interactive Front End (Siemens Corporate Research, USA), MR Echo (General Electric Healthcare, Waukesha, WI), and eXTernal Control (Philips Healthcare, Best, Netherlands).[35] In this study, we have chosen the RTHawk platform as third-party software because it can facilitate the development of MR reconstruction methods and graphic user interfaces. Applications built on the RTHawk platform can potentially be integrated with a clinical MR-guided thermal therapy system via a TCP/IP connection to transfer MRI data to other devices, thus potentially allowing for a closed-loop feedback control for hyperthermia applications.[36]

In real-time MRI, the imaging latency can be caused according to the number of baselines and coils in the pipeline. In this study, a 4-channel-spine and 8-channel-cardiac coil were used to improve the signal-to-noise ratio of MR images at a target position. We did not observe any latency for the PRFS reconstruction with 37 baselines. Further study is still needed to investigate the imaging latency with a high number of coils.

## 5. Conclusion

Abdominal organ motion due to respiration induces significant artifacts and errors on MR temperature maps. Herein we developed and evaluated an effective and practical processing pipeline for real-time, motion-robust, and multi-slice MR thermometry in abdominal organs. The proposed approach and reconstruction pipeline allowed us to perform accurate temperature measurement during free-breathing in healthy volunteers. This study lays the foundation for technological advances to achieve clinical MR-guided thermal therapy in abdominal organs successfully.

## Acknowledgments

The authors would like to thank Dr. William R. Overall at HeartVista, Inc. for assistance with developing the techniques. This study was funded by grants: NIH R21EB026018, R01EB025990, and R21CA230120.

**Conflict of interest**
The authors have no relevant conflicts of interest to declare.

**Supplemental online material**
We provided supporting materials (Figure S1-S3 and Video S1) associated with the results of the experiments in this study.

**Reference**
1. Rieke V, Pauly KB. MR thermometry. *J Magn Reson Imaging*. 2018;27(2):376-390. doi:10.1002/jmri.21265

2. Ishihara Y, Calderon A, Watanabe H, et al. A precise and fast temperature mapping using water proton chemical shift. *Magn Reson Med*. 1995;34(6):814-823. doi:10.1002/mrm.1910340606

3. De Poorter J, De Wagter C, De Deene Y, Thomsen C, Ståhlberg F, Achten E. Noninvasive MRI thermometry with the proton resonance frequency (PRF) method: in vivo results in human muscle. *Magn Reson Med*. 1995;33(1):74-81.

4. Dick EA, Gedroyc WMW. ExAblate® magnetic resonance-guided focused ultrasound system in multiple body applications. *Exp Rev Med Devices*. 2010;7(5):589-597. doi:10.1586/erd.10.38

5. Clasen S, Pereira PL. Magnetic resonance guidance for radiofrequency ablation of liver tumors. *J Magn Reson Imaging*. 2008;27(2):421-433. doi:10.1002/jmri.21264

6. Carpentier A, McNichols RJ, Stafford RJ, et al. Laser thermal therapy: real-time MRI-guided and computer-controlled procedures for metastatic brain tumors. *Lasers Surg Med*. 2011;43(10):943-950. doi:10.1002/lsm.21138

7. Oto A, Sethi I, Karczmar G, et al. MR Imaging–guided Focal Laser Ablation for Prostate Cancer: Phase I Trial. *Radiology*. 2013;267(3):932-940. doi:10.1148/radiol.13121652

8. Morikawa S, Inubushi T, Kurumi Y, et al. Feasibility of Respiratory Triggering for MR-Guided Microwave Ablation of Liver Tumors Under General Anesthesia. *CardioVasc Interv Radiol*. 2004;27(4):370-373. doi:10.1007/s00270-003-0079-9

9. Brace C. Thermal Tumor Ablation in Clinical Use. *IEEE Pulse*. 2011;2(5):28-38. doi:10.1109/MPUL.2011.942603

10. Weidensteiner C, Quesson B, Caire-Gana B, et al. Real-time MR temperature mapping of rabbit liver in vivo during thermal ablation. *Magn Reson Med*. 2003;50(2):322-330. doi:10.1002/mrm.10521

11. Stafford RJ, Dvm REP, Diederich CJ, Kangasniemi M, Olsson LE, Hazle JD.

Interleaved echo-planar imaging for fast multiplanar magnetic resonance temperature imaging of ultrasound thermal ablation therapy. *J Magn Reson Imaging*. 2004;20(4):706-714. doi:10.1002/jmri.20157

12. Fielden S, Zhao L, Miller W, et al. Spiral-based 3D MR thermometry. *J Ther Ultrasound*. 2015;3(Suppl 1):P18. doi:10.1186/2050-5736-3-S1-P18

13. Vigen KK, Daniel BL, Pauly JM, Butts K. Triggered, navigated, multi-baseline method for proton resonance frequency temperature mapping with respiratory motion. *Magn Reson Med*. 2003;50(5):1003-1010. doi:https://doi.org/10.1002/mrm.10608

14. Hey S, Maclair G, Senneville BD de, et al. Online correction of respiratory-induced field disturbances for continuous MR-thermometry in the breast. *Magn Reson Med*. 2009;61(6):1494-1499. doi:10.1002/mrm.21954

15. Pichardo S, Köhler M, Lee J, Hynnyen K. In vivo optimisation study for multi-baseline MR-based thermometry in the context of hyperthermia using MR-guided high intensity focused ultrasound for head and neck applications. *Int J Hyperthermia*. 2014;30(8):579-592. doi:10.3109/02656736.2014.981299

16. Rieke V, Vigen KK, Sommer G, Daniel BL, Pauly JM, Butts K. Referenceless PRF shift thermometry. *Magn Reson Med*. 2004;51(6):1223-1231. doi:10.1002/mrm.20090

17. Zou C, Tie C, Pan M, et al. Referenceless MR thermometry-a comparison of five methods. *Phys Med Biol*. 2017;62(1):1-16. doi:10.1088/1361-6560/62/1/1

18. Grissom WA, Rieke V, Holbrook AB, et al. Hybrid referenceless and multibaseline subtraction MR thermometry for monitoring thermal therapies in moving organs. *Med Phys*. 2010;37(9):5014-5026. doi:10.1118/1.3475943

19. Tan J, Mougenot C, Pichardo S, Drake JM, Waspe AC. Motion compensation using principal component analysis and projection onto dipole fields for abdominal magnetic resonance thermometry. *Magn Reson Med*. 2019;81(1):195-207. doi:https://doi.org/10.1002/mrm.27368

20. Maier F, Krafft AJ, Yung JP, et al. Velocity navigator for motion compensated thermometry. *Magn Reson Mater Phy*. 2012;25(1):15-22. doi:10.1007/s10334-011-0245-z

21. Svedin BT, Payne A, Parker DL. Respiration artifact correction in three-dimensional proton resonance frequency MR thermometry using phase navigators. *Magn Reson Med*. 2016;76(1):206-213. doi:10.1002/mrm.25860

22. de Senneville BD, Coupé P, Ries M, Facq L, Moonen CTW. Deep correction of breathing-related artifacts in real-time MR-thermometry. *Comput Med Imaging Graph*. 2020;87:101834. doi:10.1016/j.compmedimag.2020.101834

23. Roujol S, Ries M, Quesson B, Moonen C, Senneville BD de. Real-time MR-thermometry and dosimetry for interventional guidance on abdominal organs.

*Magn Reson Med*. 2010;63(4):1080-1087. doi:10.1002/mrm.22309

24. Celicanin Z, Auboiroux V, Bieri O, et al. Real-time method for motion-compensated MR thermometry and MRgHIFU treatment in abdominal organs. *Magn Reson Med*. 2014;72(4):1087-1095. doi:https://doi.org/10.1002/mrm.25017

25. Winter L, Oberacker E, Paul K, et al. Magnetic resonance thermometry: Methodology, pitfalls and practical solutions. *Int J Hyperthermia*. 2016;32(1):63-75. doi:10.3109/02656736.2015.1108462

26. Odéen H, Parker DL. Magnetic resonance thermometry and its biological applications – Physical principles and practical considerations. *Prog Nucl Magn Reson Spectrosc*. 2019;110:34-61. doi:10.1016/j.pnmrs.2019.01.003

27. Santos JM, Wright GA, Pauly JM. Flexible real-time magnetic resonance imaging framework. *Conf Proc IEEE Eng Med Biol Soc*. 2004;2004:1048-1051. doi:10.1109/IEMBS.2004.1403343

28. Holbrook AB, Santos JM, Kaye E, Rieke V, Pauly KB. Real-time MR thermometry for monitoring HIFU ablations of the liver. *Magn Reson Med*. 2010;63(2):365-373. doi:10.1002/mrm.22206

29. Grissom WA, Kerr AB, Holbrook AB, Pauly JM, Butts-Pauly K. Maximum Linear-Phase Spectral-Spatial RF Pulses for Fat-Suppressed PRF-Shift MR Thermometry. *Magn Reson Med*. 2009;62(5):1242-1250. doi:10.1002/mrm.22118

30. Fielden SW, Feng X, Zhao L, et al. A spiral-based volumetric acquisition for MR temperature imaging. *Magn Reson Med*. 2018;79(6):3122-3127. doi:10.1002/mrm.26981

31. Kim K, Jones P, Diederich C, Ozhinsky E. Technical Note: Low-cost MR-compatible pneumatic respiratory organ motion simulator for development of MR-guided thermal therapy. *Med Phys*. 2022;49(7):4365-4371. doi:10.1002/mp.15783

32. Boehm C, Goeger-Neff M, Mulder HT, et al. Susceptibility artifact correction in MR thermometry for monitoring of mild radiofrequency hyperthermia using total field inversion. *Magn Reson Med*. Published online 2022. doi:10.1002/mrm.29191

33. Köhler MO, Denis de Senneville B, Quesson B, Moonen CTW, Ries M. Spectrally selective pencil-beam navigator for motion compensation of MR-guided high-intensity focused ultrasound therapy of abdominal organs. *Magn Reson Med*. 2011;66(1):102-111. doi:10.1002/mrm.22784

34. Bing C, Staruch RM, Tillander M, et al. Drift correction for accurate PRF-shift MR thermometry during mild hyperthermia treatments with MR-HIFU. *Int J Hyperthermia*. 2016;32(6):673-687. doi:10.1080/02656736.2016.1179799

35. Campbell-Washburn AE, Faranesh AZ, Lederman RJ, Hansen MS. MR sequences

and rapid acquisition for MR guided interventions. *Magn Reson Imaging Clin N Am*. 2015;23(4):669-679. doi:10.1016/j.mric.2015.05.006

36. Ozhinsky E, Salgaonkar VA, Diederich CJ, Rieke V. MR thermometry-guided ultrasound hyperthermia of user-defined regions using the ExAblate prostate ablation array. *J Ther Ultrasound*. 2018;6. doi:10.1186/s40349-018-0115-5

## Figures

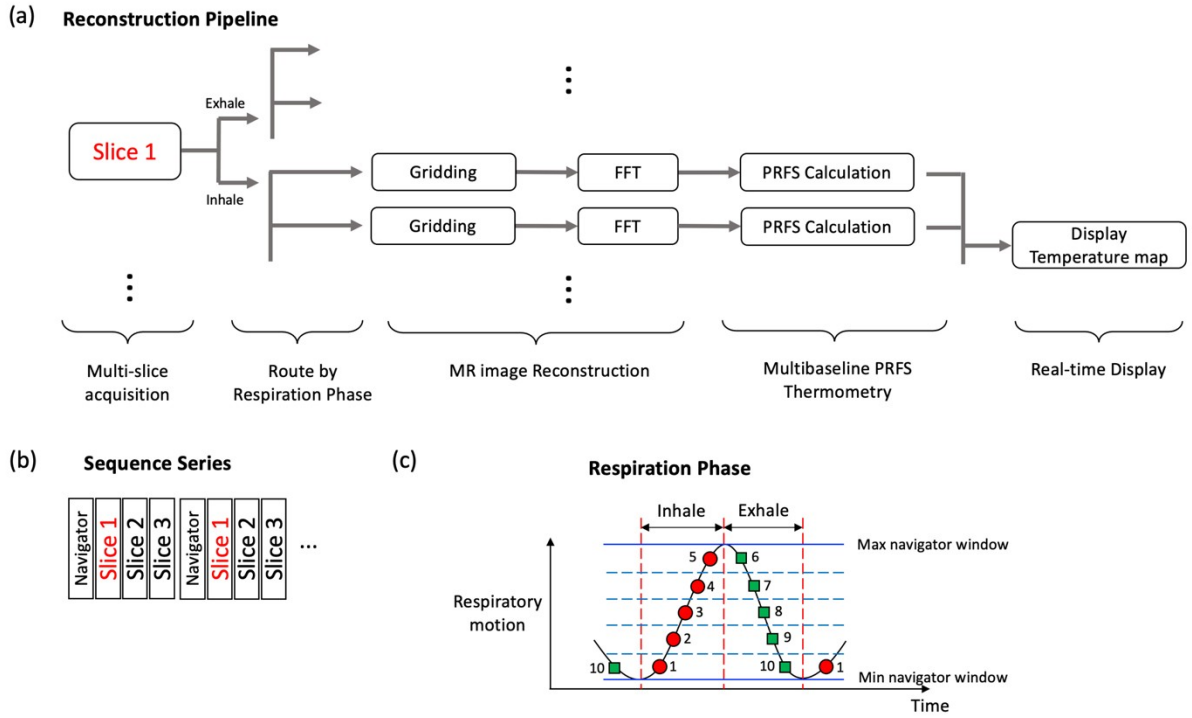


Figure *1*. (a) Multi-slice and real-time reconstruction pipeline for multi-baseline PRFS acquisition. Once MRI data is obtained, the data is sorted by a slice number, a navigator position, and a respiratory phase (inhale/exhale). (b) Interleaved acquisition sequence series and (c) an example of a multi-baseline approach: 5 baselines at each respiration phase and 10 different reference images are recorded for PRFS calculations.

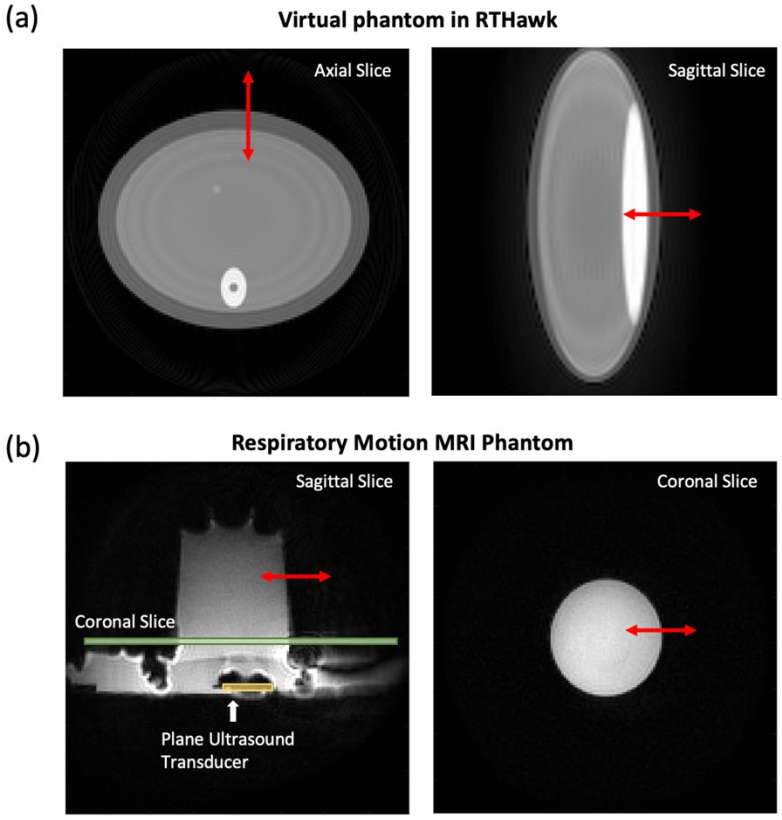


Figure *2*. MR magnitude images of (a) virtual simulation phantom and (b) respiratory motion phantom in the MRI scanner. An ultrasound transducer was set up to heat a tissue-mimicking phantom, while the motion simulator can only move the phantom. The red arrow indicates the motion direction induced by the respiratory motion.

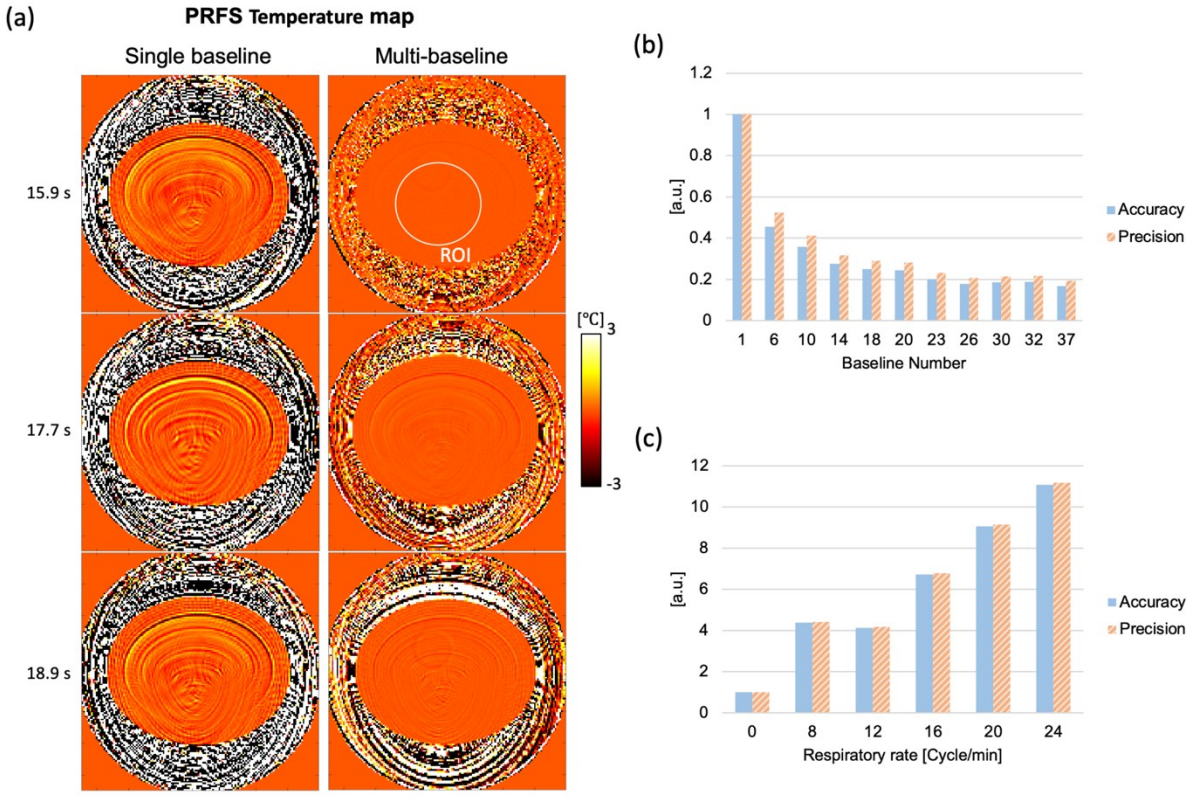


Figure 3. (a) Comparison of PRFS MR thermometry between a single baseline and multiple baselines (30 baselines) in the virtual phantom simulation. Temperature maps from multi-baseline PRFS acquisition show stable and homogeneous temperature distributions. (b-c) Bar graphs show temperature accuracy and precision according to baseline numbers and respiratory rates. In (b), respiratory rates are 12 cycles/min, and the temperature accuracy and precision in a single baseline acquisition are measured at 0.44 °C and 0.38 °C, respectively. In (c), 25 baselines are used for the PRFS reconstruction, except for no motion case (single baseline), and the temperature accuracy and precision without motion are measured at 0.0187 °C and 0.0185 °C.

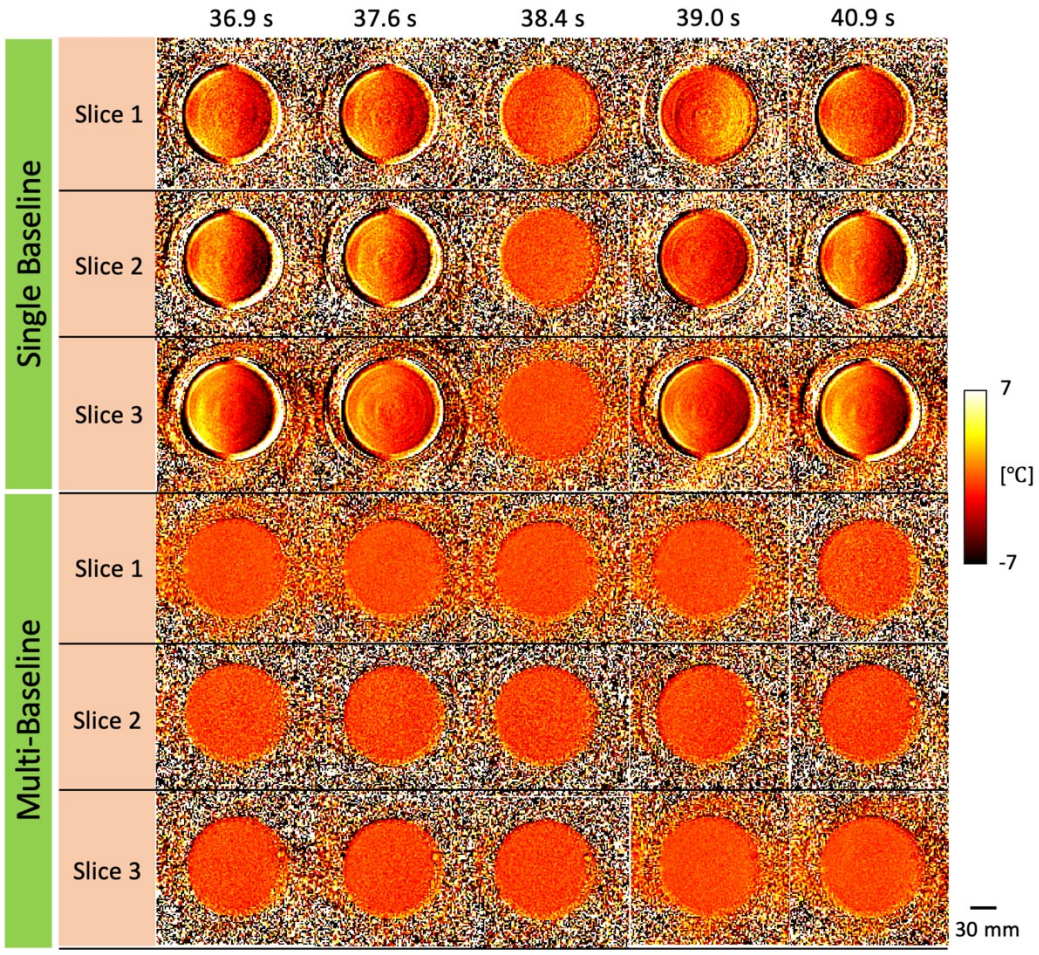


Figure 4. Time sequence of PRFS temperature maps obtained by multi-slice acquisition during the respiratory phantom experiments without ultrasound heating. A single baseline acquisition shows motion-induced artifacts in the PRFS maps, while a multi-baseline acquisition provides stable and homogeneous temperature distributions for a breathing cycle.

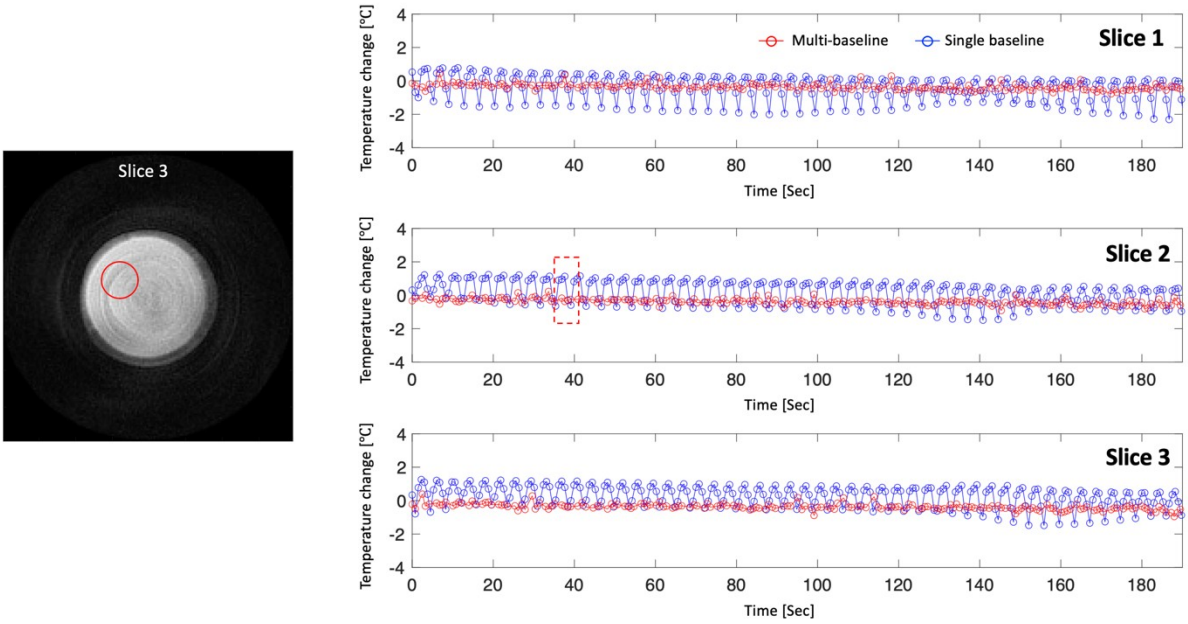


Figure 5. Time-dependent profiles from PRFS temperature maps in the respiratory phantom experiment without heating. The profiles are plotted with averaged values within an ROI (red circle, left). The red dashed box indicates a time point for temperature maps shown for slices 1, 2 and 3 in Figure 4.

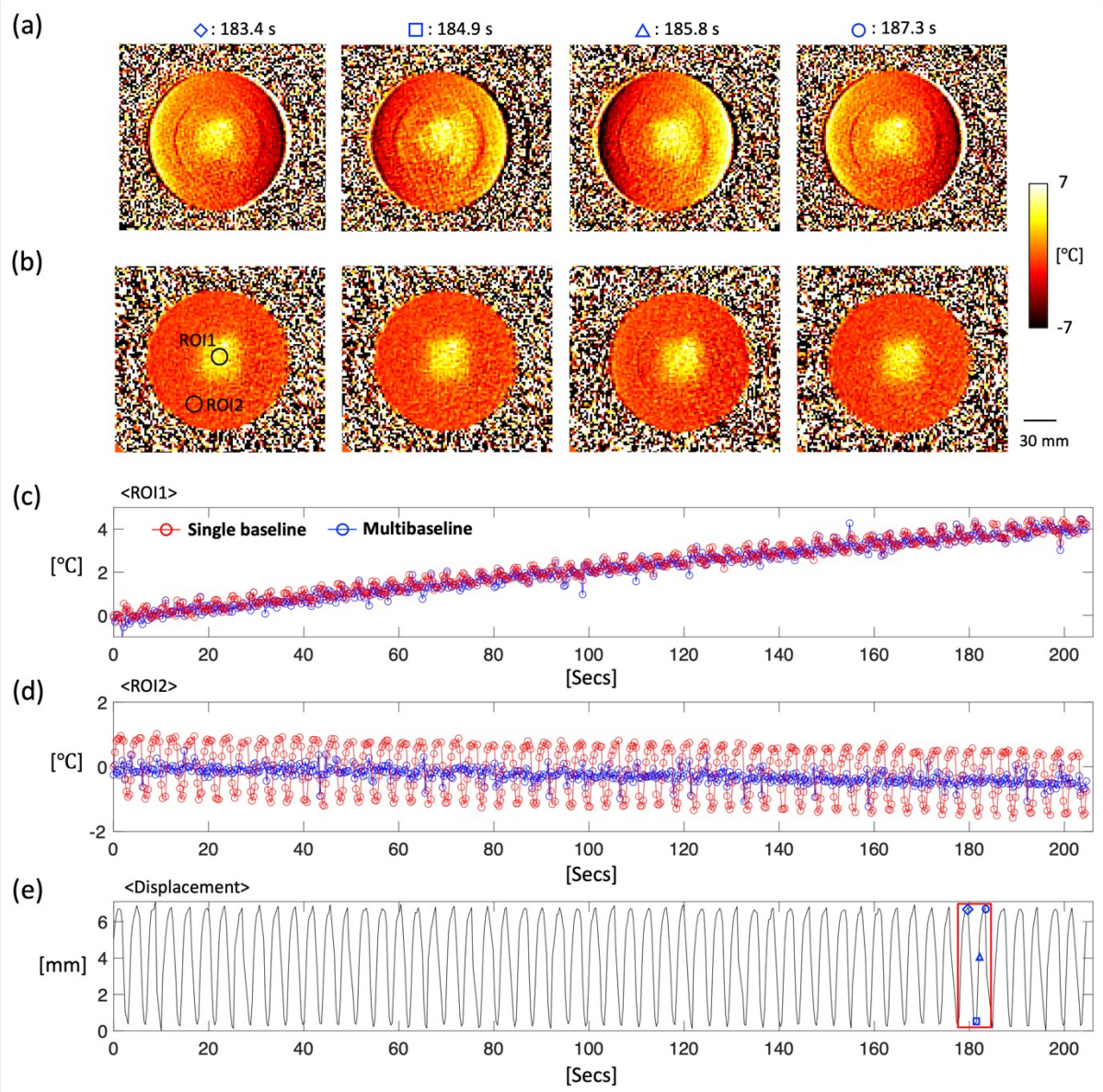


Figure 6. The results of the respiratory phantom experiment with ultrasound heating, showing PRFS temperature maps with (a) a single- and (b) a multi-baseline acquisition. More uniform heating patterns are observed in temperature maps from the multi-baseline acquisition. The profiles are plotted with averaged values within ROI 1 (c) and 2 (d), which are within and outside the heated region, respectively. In displacement records (e), the red box indicates a time point for temperature maps.

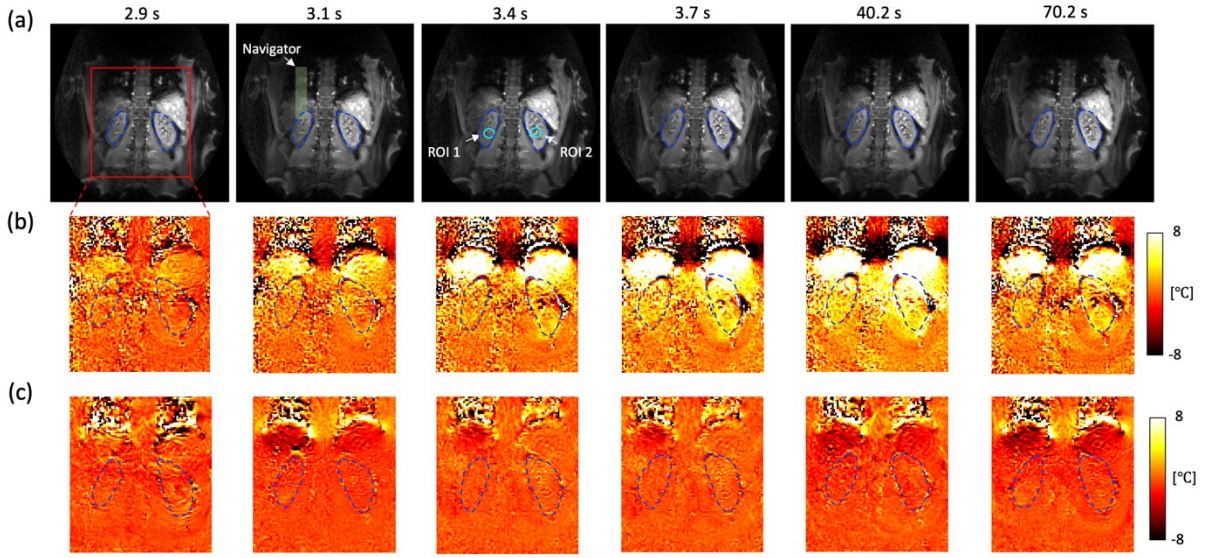


Figure 7. The result of healthy volunteer experiments without heating (volunteer #1). (a) A coronal slice is acquired and shows the left and right kidney organs which are indicated with blue dashed lines. PRFS temperature maps show that a (c) multi-baseline PRFS reconstruction allows stable and homogeneous temperature measurements, compared to a (b) single baseline (see Supporting Material Video S1). A pencil beam navigator is placed at the boundary of the diaphragm to measure a respiratory motion position.

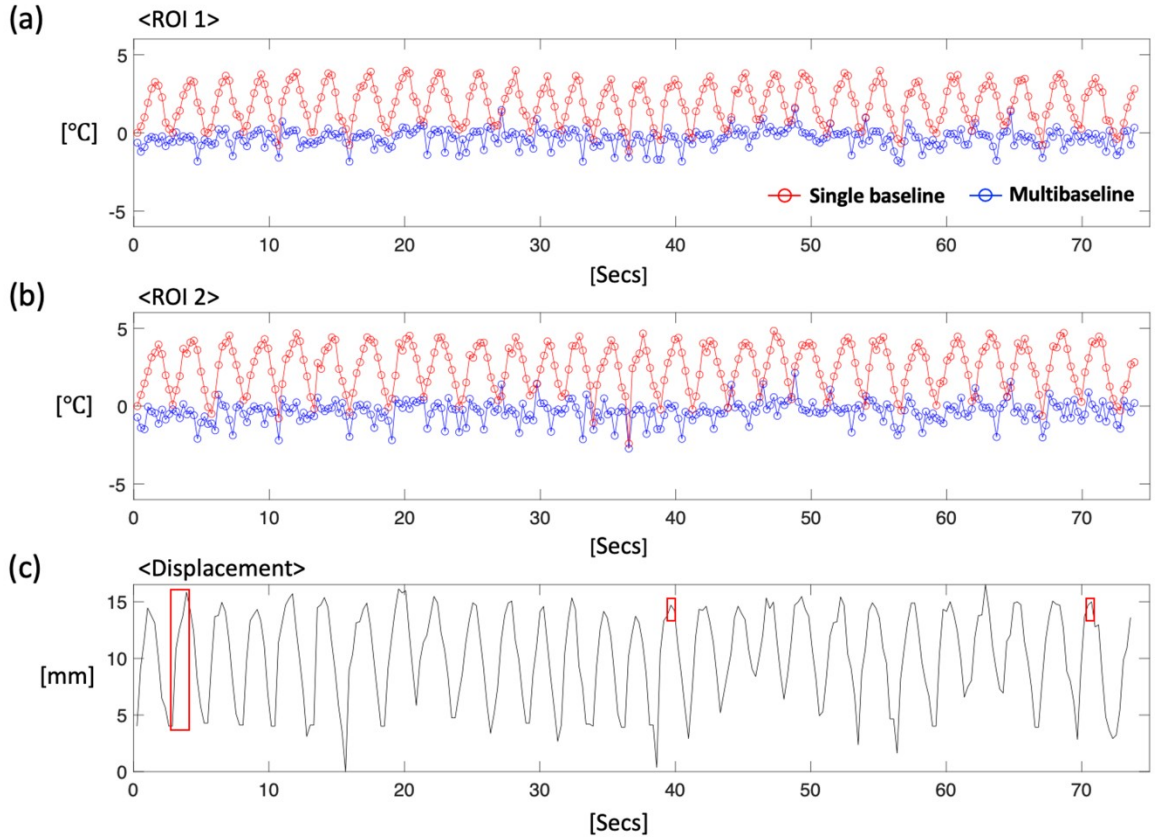


Figure 8. Time-dependent profiles within ROI 1 (a, left kidney) and ROI 2 (b, right

kidney) (volunteer #1). ROIs are shown with cyan circles in Figure 7. A single baseline reconstruction shows periodic patterns corresponding to (c) the respiratory motion, while a multi-baseline acquisition allows stable temperature measurements. The red box indicates time points for temperature maps shown in Figure 7.

**Table**

Table 1. Summary of accuracy and precision determinations for MR thermometry for all experiments in simulation, phantom, and healthy volunteers.

| Section | Subject | Baseline number | Spatial resolution [mm³] | Slice Orientation | Acquisition time per frame [ms] | Scan time [s] | Accuracy [°C] | | | Precision [°C] | | |
|---|---|---|---|---|---|---|---|---|---|---|---|---|
| 3.1 | Virtual motion phantom (12 cycles/ min) | 30 | 32.02 | Axial | 264.5 | 60 | SB | 0.44 | | SB | 0.38 | |
| | | | | | | | MB | 0.08 | | MB | 0.08 | |
| 3.2.1 | Motion phantom | 30 | 11.5 | Coronal | 713.3 per 3 slices | 190 | SB | Slice1 | 1.44 | SB | Slice1 | 1.40 |
| | | | | | | | | Slice2 | 1.16 | | Slice2 | 1.12 |
| | | | | | | | | Slice3 | 1.28 | | Slice3 | 1.11 |
| | | | | | | | MB | Slice1 | 0.84 | MB | Slice1 | 0.77 |
| | | | | | | | | Slice2 | 0.84 | | Slice2 | 0.75 |
| | | | | | | | | Slice3 | 0.81 | | Slice3 | 0.72 |
| 3.2.2 | Motion phantom (ROI 2) | 30 | 11.5 | Coronal | 303 | 205 | SB | 2.78 | | SB | 2.76 | |
| | | | | | | | MB | 1.57 | | MB | 1.51 | |

| | | | | | | | | | | |
|---|---|---|---|---|---|---|---|---|---|---|
| 3.3 | *Volunteer #1* Kidney (left) | 32 | 54.2 | Coronal | 261.2 | 74 | SB | 2.42 | SB | 2.02 |
| | | | | | | | MB | 1.02 | MB | 0.98 |
| | Volunteer #1 Kidney (right) | 32 | 54.2 | Coronal | 261.2 | | SB | 4.99 | SB | 3.49 |
| | | | | | | | MB | 1.31 | MB | 1.24 |
| | Volunteer #2 Kidney (left) | 32 | 56.2 | Axial | 261.2 | 170 | SB | 4.26 | SB | 2.43 |
| | | | | | | | MB | 1.39 | MB | 1.38 |
| | Volunteer #2 Kidney (right) | 32 | 56.2 | Axial | 261.2 | | SB | 4.42 | SB | 2.64 |
| | | | | | | | MB | 1.13 | MB | 1.10 |
| | Volunteer #2 Liver | 32 | 56.2 | Axial | 261.2 | | SB | 2.48 | SB | 1.97 |
| | | | | | | | MB | 1.10 | MB | 1.05 |
| | Volunteer #2 Liver | 32 | 40.6 | Coronal | 261.2 | 138 | SB | 7.9 | SB | 7.78 |
| | | | | | | | MB | 1.35 | MB | 1.21 |

*SB: Single Baseline (non-correction), MB: Multi-Baseline